ACCEPTED BY THE ASTROPHYSICAL JOURNAL
Preprint typeset using LaTeX style emulateapj v. 7/15/03

CHANDRA LOCALIZATIONS AND SPECTRA OF *INTEGRAL* SOURCES IN THE GALACTIC PLANE: THE CYCLE 9 SAMPLE

JOHN A. TOMSICK[1], SYLVAIN CHATY[2], JEROME RODRIGUEZ[2], ROLAND WALTER[3], PHILIP KAARET[4]

Accepted by the Astrophysical Journal

ABSTRACT

We report on 0.3–10 keV X-ray observations by the *Chandra X-ray Observatory* of the fields of 22 sources that were discovered as hard X-ray (20–100 keV) sources by the *INTEGRAL* satellite ("IGR" sources). The observations were made during *Chandra*'s 9th observing cycle, and their purpose is to localize the sources and to measure their soft X-ray spectra in order to determine the nature of the sources. We find very likely *Chandra* counterparts for 18 of the 22 sources. We discuss the implications for each source, considering previous results and new optical or IR identifications, and we identify or suggest identifications for the nature of 16 of the sources. Two of the sources, IGR J14003–6326 and IGR J17448–3232, are extended on arcminute scales. We identify the former as a pulsar wind nebula (PWN) with a surrounding supernova remnant (SNR) and the latter as a SNR. In the group of 242 IGR sources, there is only one other source that has previously been identified as a SNR. Seven of the sources are definite or candidate High-Mass X-ray Binaries (HMXBs). We confirm a previous identification of IGR J14331–6112 as an HMXB, and based on combinations of hard X-ray spectra, inferred distances and X-ray luminosities, and/or column density variations, we suggest that IGR J17404–3655, IGR J16287–5021, IGR J17354–3255, IGR J17507–2647, IGR J17586–2129, and IGR J13186–6257 are candidate HMXBs. Our results indicate or confirm that IGR J19267+1325, IGR J18173–2509, and IGR J18308–1232 are Cataclysmic Variables (CVs), and we suggest that IGR J15529–5029 may also be a CV. We confirm that IGR J14471–6414 is an Active Galactic Nucleus (AGN), and we also suggest that IGR J19443+2117 and IGR J18485–0047 may be AGN. Finally, we found *Chandra* counterparts for IGR J11098–6457 and IGR J18134–1636, but more information is required to determine the nature of these two sources.

Subject headings: stars: neutron — stars: white dwarfs — black hole physics — X-rays: stars — infrared: stars — stars: individual (IGR J07295–1329, IGR J09485–4726, IGR J11098–6457, IGR J13186–6257, IGR J14003–6326, IGR J14331–6112, IGR J14471–6414, IGR J15529–5029, IGR J16287–5021, IGR J17354–3255, IGR J17404–3655, IGR J17448–3232, IGR J17461–2204, IGR J17487–3124, IGR J17507–2647, IGR J17586–2129, IGR J18134–1636, IGR J18173–2509, IGR J18308–1232, IGR J18485–0047, IGR J19267+1325, IGR J19443+2117)

1. INTRODUCTION

The *International Gamma-Ray Astrophysics Satellite (INTEGRAL)* (Winkler et al. 2003) has been in operation for more than six years and has discovered a large number of new hard X-ray sources at energies >20 keV. This bandpass is above the range where most types of sources can emit thermal blackbody radiation. Thus, *INTEGRAL* provides a window on the non-thermal emission that comes from Galactic sources (e.g., accreting black holes, neutron stars, and magnetized white dwarfs) as well as extragalactic Active Galactic Nuclei (AGN). With large field-of-view (FOV) coded aperture mask instruments (e.g., a $29^\circ \times 29^\circ$ partially coded FOV for IBIS, Lebrun et al. 2003; Ubertini et al. 2003), *INTEGRAL* has observed most of the sky thus far during its mission, but its sky coverage has not been uniform, with more time being concentrated near the Galactic plane. While IBIS has provided a step forward in hard X-ray angular resolution, it localizes 20–40 keV sources to 1–5′, which is normally not sufficient to identify an optical or infrared counterpart, leaving the nature of many of the sources uncertain. Thus, throughout the *INTEGRAL* mission, follow-up observations have been made with soft X-ray (∼0.5–10 keV) telescopes (*Chandra*, *XMM-Newton*, and *Swift*) to localize the *INTEGRAL* sources and determine their nature.

As of 2009 March, *INTEGRAL* had detected nearly 600 sources, and 242 of these are IGR sources[5], being either newly discovered by *INTEGRAL* or not previously detected in the ∼20–100 keV band (see Bodaghee et al. 2007, for more on the criterion for the IGR classification). The source types of the 242 IGR sources are dominated by 79 AGN (73 with firm identifications), 67 X-ray binaries (47 with firm identifications), and 15 Cataclysmic Variables (CVs). There are small numbers of IGR sources in a few other categories (Symbiotic stars, active stars, an Anomalous X-ray Pulsar, and a Supernova Remnant), and the remaining 72 IGR sources are unclassified. Along with the soft X-ray localizations (e.g., Tomsick et al. 2006, 2008b), the steady increase in the numbers of classified IGR sources depends on ground-based optical and IR follow-up observations (e.g., Masetti et al. 2008,

[1] Space Sciences Laboratory, 7 Gauss Way, University of California, Berkeley, CA 94720-7450, USA (e-mail: jtomsick@ssl.berkeley.edu)
[2] AIM - Astrophysique Interactions Multi-échelles (UMR 7158 CEA/CNRS/Université Paris 7 Denis Diderot), CEA Saclay, DSM/IRFU/Service d'Astrophysique, Bât. 709, L'Orme des Merisiers, FR-91 191 Gif-sur-Yvette Cedex, France
[3] INTEGRAL Science Data Centre, Observatoire de Genève, Université de Genève, Chemin d'Ecogia, 16, 1290 Versoix, Switzerland
[4] Department of Physics and Astronomy, University of Iowa, Iowa City, IA 52242, USA

[5] See http://isdc.unige.ch/∼rodrigue/html/igrsources.html for a continually updated list of IGR sources.

2009; Chaty et al. 2008; Butler et al. 2009), which are key to obtaining firm identifications.

One of the most interesting categories of IGR sources are the High-Mass X-ray Binaries (HMXBs), for which *INTEGRAL* has uncovered two new (and not entirely independent) classes: The obscured HMXBs (Walter et al. 2003; Matt & Guainazzi 2003; Walter et al. 2006) and the Supergiant Fast X-ray Transients (SFXTs, Negueruela et al. 2006; Sguera et al. 2006; Walter & Zurita Heras 2007). The obscured HMXBs have large and, in some cases, variable levels of intrinsic (i.e., local) absorption with $N_{\rm H} \sim 10^{23-24}$ cm^{-2}. There is evidence in several cases that a strong stellar equatorial outflow is responsible for the absorption, including the detection of P Cygni profiles (Filliatre & Chaty 2004; Chaty et al. 2008), providing direct evidence for a wind, as well as excess emission in the mid-infrared (Rahoui et al. 2008). The strong winds and high absorption explain why *INTEGRAL*'s hard X-ray imaging was necessary to detect these sources, and it has been suggested that these obscured HMXBs are in a previously unstudied phase of HMXB evolution (Lommen et al. 2005). With the discovery of SFXTs, *INTEGRAL* found a new type of HMXB behavior where sources undergo high-amplitude (orders of magnitude) hard X-ray flares that only last for time scales of hours (in't Zand 2005; Sguera et al. 2006). In part, this is thought to be caused by clumps in the supergiant stellar winds (Walter & Zurita Heras 2007), but it may also be related to the interaction between the wind and a strong neutron star magnetic field (Bozzo, Falanga & Stella 2008).

To identify the nature of more of these sources, we have been using *Chandra* to study the unclassified IGR sources near the Galactic plane. The primary purpose of the observations is to localize the sources to allow for optical or IR follow-up. While X-ray positions with an accuracy of several arcseconds (as can be given by *Swift* or *XMM-Newton*) can lead to correct optical or IR identifications, in many cases (and especially in the crowded regions of the Galactic plane), the sub-arcsecond *Chandra* positions are crucial for obtaining definitive identifications. A second important use for the *Chandra* observations is to measure the soft X-ray energy spectrum, providing information about source hardness and levels of absorption that help to determine the nature of the source. Our *Chandra* program began in 2005 with the identification of 4 IGR sources (Tomsick et al. 2006), and we subsequently used *Chandra* observations taken between 2007 and 2008 to obtain identifications for 12 more IGR sources (Tomsick et al. 2008a). In this work, we report on 22 *Chandra* observations taken during *Chandra*'s 9th observing cycle between late-2007 and early-2009.

2. *CHANDRA* OBSERVATIONS

For *Chandra* follow-up observations, we chose sources from the 27th *INTEGRAL* General Reference Catalog[6] that were detected in the 20–40 keV band as of 2007 March. The list that we produced includes IGR sources within 5° of the Galactic plane, and we used information from Bird et al. (2006) and Bodaghee et al. (2007) to select sources that were not known to be transient and whose nature was unknown at the time. Ultimately, we chose the 22 sources listed in Table 1 for ∼5 ks "snapshot" observations with *Chandra* to provide precise X-ray localizations as well as information about their soft X-ray spectra.

[6] See http://isdc.unige.ch/Data/cat.

As listed in Table 1, the observations were made between 2007 November and 2009 February, and we used the Advanced CCD Imaging Spectrometer (ACIS, Garmire et al. 2003). The 90% confidence *INTEGRAL* error circles range from 2′.2 to 5′.4, leading us to use the 16.9×16.9 arcmin^2 field-of-view (FOV) of the ACIS-I instrument. Our analysis of the ACIS data began by downloading the most recent versions of the data products as of 2009 January-February. We started with the "level 1" data files, and these were processed at the *Chandra* X-Ray Center with pipeline ("ASCDS") versions 7.6.11.2 to 7.6.11.9. We performed further processing with the *Chandra* Interactive Analysis of Observations (CIAO) version 4.1.1 (except for one part of the analysis as mentioned below) software. Also, we used version 4.1.1 of the Calibration Data Base (CALDB). We used the CIAO routine `acis_process_events` to produce the "level 2" event lists that we used to make images and energy spectra. While a level 2 file is provided as part of the standard data pipeline, we re-produced the file in order to use the most recent time-dependent gain information. With a current version of the CALDB, using the CIAO 4.1.1 default parameters when running `acis_process_events` incorporates the most recent calibration files.

3. ANALYSIS AND RESULTS

3.1. *Search for Sources and X-ray Identifications*

After producing 0.3–10 keV images, we used the CIAO routine `wavdetect` to search for X-ray sources on the ACIS-I chips. Although we originally used the version of `wavdetect` found in CIAO 4.1.1, we noticed that many spurious detections (sources with one or two photons) occurred for some of the observations. However, these spurious detections did not occur with CIAO 3.4, and we used that version of `wavdetect` for the source searches in this paper. For each observation, we searched for sources in unbinned images with 2048×2048 pixels as well as images binned by a factor of 2 (1024×1024 pixels) and a factor of 4 (512×512 pixels). In each case, we set the detection threshold to a level that would be expected to yield one spurious source (2.4×10^{-7}, 9.5×10^{-7}, and 3.8×10^{-6} for the three images, respectively). Thus, in the merged lists of detected sources, it would not be surprising if a few of the sources in each field are spurious.

The average number of sources detected per observation over the entire ACIS-I FOV is 20, with the minimum being 12 sources and the maximum being 32 sources. We used 3 main criteria to determine which of these are likely counterparts to the IGR sources. First, the IGR sources have been detected by *INTEGRAL* at 20–40 keV flux levels of 0.5–2 millicrab (Bird et al. 2006). At 1 millicrab (20–40 keV), a source with an absorbed power-law spectrum with a photon index of $\Gamma = 1.0$ and a column density of $N_{\rm H} = 5 \times 10^{22}$ cm^{-2} would yield ∼300 ACIS-I counts in 5 ks, so we are looking for fairly bright *Chandra* sources. Second, the sources should have hard spectra, and third, the sources should be within or close to the *INTEGRAL* error circles.

We estimated the hardness of each of the detected *Chandra* sources by determining the number of source counts in the 0.3–2 keV band (C_1) and the 2–10 keV band (C_2). Using the size of the *Chandra* point spread function (PSF) as a guide, we used extraction radii of 5″ for sources within 4′ of the aimpoint, 10″ for sources between 4′ and 7′ from the aimpoint, and 15″ for sources more than 7′ from the aimpoint. The background counts were taken from the largest possible rectangular source-free region, and this value was scaled to

TABLE 1
Chandra OBSERVATIONS

IGR Name	ObsID	l^a	b^b	Start Time	Exposure Time (s)
J07295–1329	9061	228.97	+2.26	2008 Feb 11, 0.55 h UT	5093
J09485–4726	9068	273.84	+4.84	2007 Nov 30, 19.98 h UT	5055
J11098–6457	9066	292.43	–4.17	2008 Sept 12, 14.66 h UT	5109
J13186–6257	9049	306.02	–0.24	2008 Sept 11, 22.14 h UT	5061
J14003–6326	9058	310.57	–1.61	2008 June 29, 12.13 h UT	5077
J14331–6112	9053	314.90	–0.72	2008 Jan 5, 4.39 h UT	4888
J14471–6414	9065	315.00	–4.15	2007 Dec 27, 7.83 h UT	5112
J15529–5029	9062	329.89	+2.63	2008 Jan 7, 8.58 h UT	5071
J16287–5021	9054	334.16	–1.13	2008 Jan 28, 10.84 h UT	4935
J17354–3255	9050	355.44	–0.26	2009 Feb 6, 7.15 h UT	4692
J17404–3655	9063	352.64	–3.27	2008 July 16, 21.02 h UT	4894
J17448–3232	9059	356.84	–1.76	2008 Nov 2, 2.15 h UT	4692
J17461–2204	9064	5.94	+3.48	2009 Feb 6, 5.27 h UT	4888
J17487–3124	9060	358.25	–1.83	2008 Nov 2, 0.33 h UT	4888
J17507–2647	9048	2.42	+0.15	2009 Feb 6, 8.79 h UT	4698
J17586–2129	9056	8.05	+1.35	2008 Oct 30, 3.38 h UT	4888
J18134–1636	9052	13.88	+0.61	2008 Feb 16, 9.52 h UT	4891
J18173–2509	9067	6.79	–4.26	2008 May 6, 1.15 h UT	4894
J18308–1232	9055	19.45	–1.19	2008 Apr 27, 16.69 h UT	4698
J18485–0047	9051	31.90	+0.31	2008 Apr 27, 14.97 h UT	4695
J19267+1325	9075	48.88	–1.53	2008 Feb 27, 2.46 h UT	4698
J19443+2117	9057	57.79	–1.37	2008 Feb 27, 0.68 h UT	4888

[a]Galactic longitude in degrees.
[b]Galactic latitude in degrees.

the size of the source extraction region and subtracted off. We then calculated the hardness according to $(C_2-C_1)/(C_2+C_1)$, which runs from –1.0 for the softest sources (all the counts in the 0.3–2 keV band) to +1.0 for the hardest sources (all the counts in the 2–10 keV band). To deal with the case where there are zero counts in one of the energy bands, we used the "Gehrels" prescription for determining the uncertainties (Gehrels 1986).

Figure 1 shows a hardness-intensity diagram, including all 434 of the sources detected. For most sources with fewer than $\sim$10 counts, the uncertainties on the hardnesses are very large. However, one can see a group of 19 sources with more than 100 counts per source and hardnesses greater than zero, and we consider these as candidate counterparts to the IGR sources. In addition to the 19 sources, we also consider a 20th source that only has 29 counts, but its hardness is 1.0 ± 0.3, and it is well within the *INTEGRAL* error circle for IGR J13186–6257. Thus, we consider these 20 sources as candidate counterparts. While 18 of these sources are consistent with being point sources, two of the sources (marked with diamonds in Figure 1) are clearly extended. The *Chandra* positions, numbers of ACIS-I counts in the 0.3–10 keV band, and hardness ratios (using the definition given above) for the 20 sources are given in Table 2. The 20 sources come from 18 different observations. The candidate counterparts for 16 of the IGR sources are unique, and in two cases (IGR J17354–3255 and IGR J17448–3232), there are 2 possible counterparts. In §3.3, we estimate the probability of spurious *Chandra*/IGR source associations. For the other 4 IGR sources (IGR J07295–1329, IGR J09485–4726, IGR J17461–2204, and IGR J17487–3124), there are no strong possibilities for counterparts. However, *Chandra* sources are detected in each of these 4 fields as well, and *Chandra* source lists can be found in the on-line tables associated with this paper (see Appendix).

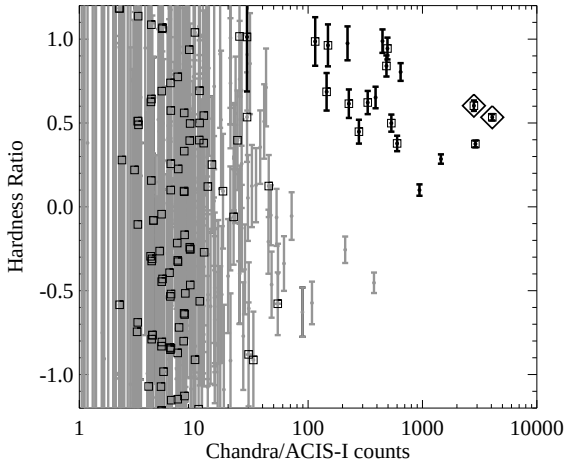

FIG. 1.— Hardness-intensity diagram, including all of the *Chandra*/ACIS-I sources detected in the 22 *Chandra* observations. The intensity is given as the number of ACIS-I counts in the 0.3–10 keV energy band. The hardness is given by $(C_2-C_1)/(C_2+C_1)$, where C_1 is the number of counts in the 0.3–2 keV band and C_2 is the number of counts in the 2–10 keV band. The squares indicate sources that are inside their respective 90% confidence *INTEGRAL* error circles. The sources that we consider as possible *Chandra* counterparts to the IGR sources are plotted with black points and error bars. The two sources marked with diamonds are extended sources.

3.2. *Spectral Analysis of Point Sources*

We produced *Chandra* energy spectra for the 18 point source candidate counterparts using the CIAO software routines. We used the same source extraction regions described above for determining count rates and hardnesses. For the

TABLE 2
Chandra CANDIDATE COUNTERPARTS TO IGR SOURCES

CXOU Name	θ (arcminutes)[a]	*Chandra* R.A. (J2000)[b]	*Chandra* Decl. (J2000)[b]	ACIS Counts	Hardness Ratio
IGR J11098-6457, *INTEGRAL* error radius = 5.5 arcmin[c]					
J110926.4–650224	6.02	$11^h09^m26^s.43$	$-65°02'25''.0$	941.2	0.10 ± 0.03
IGR J13186–6257, *INTEGRAL* error radius = 3.8 arcmin[c]					
J131825.0–625815	1.94	$13^h18^m25^s.08$	$-62°58'15''.5$	29.3	1.01 ± 0.33
IGR J14003–6326, *INTEGRAL* error radius = 3.9 arcmin[c]					
J140045.6–632542[d]	1.47	$14^h00^m45^s.69$	$-63°25'42''.6$	4075.5	0.53 ± 0.02
IGR J14331–6112, *INTEGRAL* error radius = 3.7 arcmin[c]					
J143308.3–611539	4.02	$14^h33^m08^s.33$	$-61°15'39''.9$	644.1	0.80 ± 0.05
IGR J14471–6414, *INTEGRAL* error radius = 4.6 arcmin[c]					
J144628.2–641624	1.46	$14^h46^m28^s.26$	$-64°16'24''.1$	600.3	0.38 ± 0.05
IGR J15529–5029, *INTEGRAL* error radius = 3.9 arcmin[c]					
J155246.9–502953	1.59	$15^h52^m46^s.92$	$-50°29'53''.4$	278.3	0.45 ± 0.07
IGR J16287–5021, *INTEGRAL* error radius = 4.4 arcmin[c]					
J162826.8–502239	3.12	$16^h28^m26^s.85$	$-50°22'39''.7$	484.3	0.84 ± 0.06
IGR J17354–3255, *INTEGRAL* error radius = 2.2 arcmin[c]					
J173518.7–325428	1.83	$17^h35^m18^s.73$	$-32°54'28''.7$	145.2	0.69 ± 0.11
J173527.5–325554	1.34	$17^h35^m27^s.59$	$-32°55'54''.4$	494.2	0.94 ± 0.07
IGR J17404–3655, *INTEGRAL* error radius = 3.5 arcmin[c]					
J174026.8–365537	0.84	$17^h40^m26^s.86$	$-36°55'37''.4$	227.3	0.62 ± 0.09
IGR J17448–3232, *INTEGRAL* error radius = 2.2 arcmin[c]					
J174453.4–323254[d]	0.33	$17^h44^m53^s.44$	$-32°32'54''.1$	2816.3	0.60 ± 0.03
J174437.3–323222	3.77	$17^h44^m37^s.34$	$-32°32'23''.0$	389.0	0.65 ± 0.06
IGR J17507–2647, *INTEGRAL* error radius = 2.6 arcmin[c]					
J175039.4–264436	2.97	$17^h50^m39^s.47$	$-26°44'36''.2$	221.1	0.98 ± 0.10
IGR J17586–2129, *INTEGRAL* error radius = 3.3 arcmin[c]					
J175834.5–212321	3.81	$17^h58^m34^s.56$	$-21°23'21''.6$	447.2	0.99 ± 0.07
IGR J18134–1636, *INTEGRAL* error radius = 3.8 arcmin[c]					
J181328.0–163548	0.97	$18^h13^m28^s.03$	$-16°35'48''.5$	149.2	0.96 ± 0.13
IGR J18173–2509, *INTEGRAL* error radius = 2.2 arcmin[c]					
J181722.1–250842	0.86	$18^h17^m22^s.18$	$-25°08'42''.5$	332.2	0.62 ± 0.07
IGR J18308–1232, *INTEGRAL* error radius = 3.3 arcmin[c]					
J183049.9–123219	0.83	$18^h30^m49^s.95$	$-12°32'19''.1$	534.3	0.50 ± 0.05
IGR J18485–0047, *INTEGRAL* error radius = 3.4 arcmin[c]					
J184825.4–004635	0.55	$18^h48^m25^s.47$	$-00°46'35''.2$	115.3	0.99 ± 0.15
IGR J19267+1325, *INTEGRAL* error radius = 3.7 arcmin[c]					
J192626.9+132205	4.79	$19^h26^m26^s.99$	$+13°22'05''.1$	1450.3	0.29 ± 0.03
IGR J19443+2117, *INTEGRAL* error radius = 4.9 arcmin[c]					
J194356.2+211823	4.88	$19^h43^m56^s.23$	$+21°18'23''.6$	2902.2	0.38 ± 0.02

[a]The angular distance between the center of the *INTEGRAL* error circle, which is also the approximate *Chandra* aimpoint, and the source.
[b]The position uncertainties for these relatively bright sources are dominated by the systematic error, which is $0''.64$ at 90% confidence and $1''$ at 99% confidence (Weisskopf 2005).
[c]These are the 90% confidence errors given in Bird et al. (2006).
[d]Extended source.

background, we used rectangular source-free regions as described above, but they were modified so that they would include counts from only the ACIS-I CCD chip that also includes the source. There are 4 ACIS-I CCD chips, and in some cases, the spacecraft dithering causes source counts to be spread across multiple CCD chips. In this case, we put the background region on the CCD chip containing the largest number of source counts. Once the source and background regions were determined, we used the CIAO routine `dmextract` to produce energy spectra and `mkacisrmf` and `mkarf` to produce the response files for the source region. In the cases where the source counts are spread over multiple CCD chips, we used a weight map to produce weighted response files.

We fitted the 0.3–10 keV ACIS spectra using the XSPEC v12 software. Initially, we rebinned the spectra to 13 energy bins prior to fitting with an absorbed power-law model using χ^2-minimization in order to be able to see if and how the spectra deviate from this basic model. To account for absorption, we used the photoelectric absorption cross sections from Balucinska-Church & McCammon (1992) and elemental abundances from Wilms, Allen & McCray (2000), which correspond to the estimated abundances for the interstellar medium. For 12 of the 18 point sources, no pattern in the residuals to the absorbed power-law are apparent, and the reduced-χ^2 values in these cases range from χ^2_ν = 0.22 to 1.5 for 10 degrees of freedom (dof). For 5 of the remaining sources (CXOU J144628.2–641624, CXOU J173527.5–325554, CXOU J181722.1–250842, CXOU J183049.9–123219, and CXOU J194356.2+211823), a high energy excess is present above $\sim$7 keV, which most likely indicates that the spectra are affected by pile-up. We confirmed that pile-up is the most likely explanation by looking at the numbers of counts above 10 keV for all 18 spectra. Although ACIS has

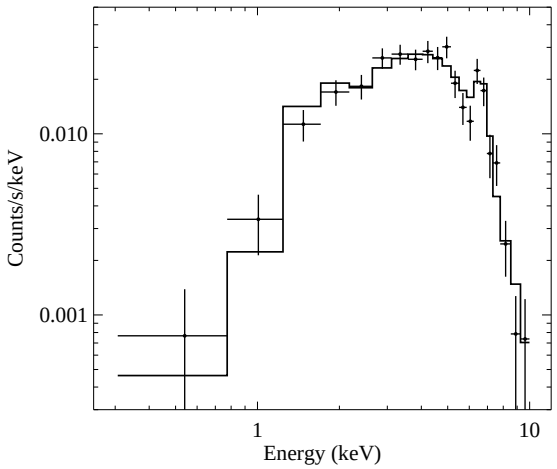

FIG. 2.— *Chandra* spectrum for CXOU J143308.3–611539 (= IGR J14331–6112), which has been confirmed as a High-Mass X-ray Binary based on optical spectroscopy. The X-ray spectrum is fitted with an absorbed power-law continuum and a Gaussian iron line with an equivalent width of ∼945 eV.

very little sensitivity above 10 keV, these 5 sources have 12, 22, 18, 22, and 24 counts at >10 keV compared to an average of 4 counts at >10 keV for the other 13 sources. In addition, adding the Davis (2001) pile-up model to the spectral model significantly improves the fits for the 5 piled-up spectra.

Thus, after accounting for pile-up, 17 of the 18 sources are consistent with a power-law model with various levels of absorption. The one source that is not consistent with a power-law is CXOU J143308.3–611539, for which $\chi^2_\nu = 2.5$ for 10 dof, and its residuals show a large excess in the energy bin corresponding to the Fe Kα transition energy. This likely indicates the presence of an Fe emission line, and adding a Gaussian with an energy of $E_{\rm line} = 6.70^{+0.25}_{-0.17}$ keV, a width of $\sigma_{\rm line} = 0.27^{+0.21}_{-0.14}$ keV, and a flux of $N_{\rm line} = (7.0^{+4.8}_{-3.4}) \times 10^{-5}$ photons cm^{-2} s^{-1} improves the quality of the fit to $\chi^2_\nu = 1.0$ for 7 dof. Figure 2 shows the *Chandra* spectrum (rebinned to 21 bins rather than 13 bins) for CXOU J143308.3–611539, and the presence of the iron line, which has a very large equivalent width of 945 eV, is clear.

After determining the spectral models with the binned spectra, we refitted all 18 of the spectra using Cash statistics (Cash 1979) and unbinned spectra, which have 663 bins after restricting the energy range to 0.3–10 keV. The best fit parameters with 90% confidence errors are given in Table 3 along with the Galactic $N_{\rm H}$ and $N_{\rm H_2}$ values for each source (Kalberla et al. 2005; Dame, Hartmann & Thaddeus 2001). The column densities measured by *Chandra* range from being significantly less than the Galactic values to being consistent with sources that are extremely absorbed ($\sim 10^{23-24}$ cm^{-2}). To determine which spectra show evidence for absorption by material local to the source, Table 3 includes limits on local absorption for each source. In each case, the upper limit of this quantity, $N_{\rm H,local}$, is the upper end of the 90% confidence error region for the column density measured by *Chandra*, while the lower limit is given by the lower end of this error region minus the maximum absorption that could be interstellar ($N_{\rm H} + 2N_{\rm H_2}$, where these are the Galactic values). Figure 3 shows the spectra for the six sources that show the highest measured values of $N_{\rm H}$. The sources CXOU J131825.0–625815, CXOU J175834.5–212321, CXOU J181328.0–163548, and CXOU J184825.4–004635 require local absorption at the 90% confidence level with $N_{\rm H,local}$ ranges of (2–84)$\times 10^{22}$ cm^{-2}, (9–22)$\times 10^{22}$ cm^{-2}, (4–17)$\times 10^{22}$ cm^{-2}, and (41–96)$\times 10^{22}$ cm^{-2}. The other two sources, CXOU J173527.5–325554 and CXOU J175039.4–264436 may or may not have significant levels of local absorption with upper limits on $N_{\rm H,local}$ of $<1.1 \times 10^{23}$ cm^{-2} and $<2.1 \times 10^{23}$ cm^{-2}, respectively.

3.3. *Using X-ray Source Number Densities to Assess the Probability of Spurious Associations*

With the spectral parameters for the point sources determined, we can now calculate the probability that the candidate associations between the *Chandra* and IGR sources are spurious. This calculation requires knowledge of the number density of X-ray sources with fluxes between $\sim 10^{-13}$ and $\sim 10^{-11}$ ergs cm^{-2} s^{-1} in the Galactic plane. The broadest survey to date that resulted in a suitable $\log N$-$\log S$ curve was done by the *Advanced Satellite for Cosmology and Astrophysics (ASCA)*. The survey covers Galactic longitudes from –45° to +45° and Galactic latitudes from –0.4° to +0.4°. The 2–10 keV $\log N$-$\log S$ is described as a power-law with $N(> F_{2-10\ \rm keV}) = 9.2(F_{2-10\ \rm keV}/10^{-13})^{-0.79}$ deg^{-2}, where $F_{2-10\ \rm keV}$ is the absorbed 2–10 keV flux in units of ergs cm^{-2} s^{-1} (Sugizaki et al. 2001). The flux range for the *ASCA* survey is 2×10^{-13} to 10^{-10} ergs cm^{-2} s^{-1} (2–10 keV). Smaller surveys of parts of the Galactic plane by *XMM-Newton* and *Chandra* that extend the $\log N$-$\log S$ to lower flux levels give $\log N$-$\log S$ curves that are consistent with *ASCA* in the flux ranges where they overlap (Hands et al. 2004; Ebisawa et al. 2005).

To calculate the probabilities of spurious associations, we first used the spectral parameters for the 18 *Chandra* point source (see Table 3) to determine the absorbed 2–10 keV flux for each source, and these are reported in Table 4. Then, we used the source density expression given above to calculate $N(> F_{2-10\ \rm keV})$ for each source. To determine the area in which we searched to find the *Chandra* source, we consider both the angular distance of the *Chandra* source from the center of the *INTEGRAL* error circle (θ in Table 4) and the radius of the 90% confidence *INTEGRAL* error circle ($\theta_{INTEGRAL}$ in Table 4), and we used the larger of these two quantities to calculate the probability.

As shown in Table 4, this analysis indicates a probability of a spurious association of <1% in 14 cases and in the 1–2% range in 3 cases. The faintest of the sources, CXOU J131825.0–625815, is the only one with an appreciable probability of a spurious association at 5.4%. While this could indicate that the association is spurious, the calculation does not account for the fact that the source is a hard X-ray source and also that it is relatively close to the center of the *INTEGRAL* error circle. One other case to consider is that of IGR J17354–3255, for which we found two *Chandra* sources within the *INTEGRAL* error circle. Although it is possible that both sources contribute to the flux detected by *INTEGRAL*, it is still probably most reasonable to consider that one of these is a spurious association. While CXOU J131825.0–625815, CXOU J173518.7–325428, CXOU J173527.5–325554 would be the leading candidates for being spurious associations, the results of these calculations increase our confidence in the associations between the *Chandra* and IGR sources.

TABLE 3
Chandra SPECTRAL RESULTS

CXOU Name	$N_{\rm H}$ ($\times10^{22}$ cm^{-2})[a]	Γ[a]	X-ray Flux[b]	α[c]	Fit Statistic[d]	Galactic $N_{\rm H}/N_{\rm H_2}$ ($\times10^{22}$ cm^{-2})[e]	$N_{\rm H,local}$ ($\times10^{22}$ cm^{-2})[f]
J110926.4–650224	$0.65^{+0.18}_{-0.17}$	1.43 ± 0.17	$4.8^{+0.4}_{-0.3}$	–	530.6/660	0.52/0.085	<0.83
J131825.0–625815	18^{+66}_{-13}	$1.9^{+6.3}_{-2.0}$	$1.0^{+47.9}_{-0.6}$	–	149.2/660	1.26/0.95	2–84
J143308.3–611539[g]	$2.2^{+0.9}_{-0.8}$	$0.34^{+0.37}_{-0.33}$	$6.3^{+0.7}_{-0.6}$	–	614.2/657	1.51/0.53	<3.1
J144628.2–641624	$1.21^{+0.22}_{-0.40}$	$1.50^{+0.20}_{-0.45}$	$7.1^{+1.8}_{-0.6}$	$1.0^{+0.0}_{-0.6}$	653.5/659	0.38/0.00	0.4–1.4
J155246.9–502953	$0.59^{+0.41}_{-0.25}$	$0.60^{+0.30}_{-0.28}$	$1.8^{+0.3}_{-0.2}$	–	522.0/660	0.68/0.050	<1.0
J162826.8–502239	$0.35^{+0.90}_{-0.35}$	$-0.82^{+0.32}_{-0.26}$	$6.8^{+0.9}_{-0.8}$	–	637.0/660	1.37/0.45	<1.3
J173518.7–325428	$2.6^{+1.4}_{-1.2}$	$0.79^{+0.56}_{-0.53}$	$1.44^{+0.26}_{-0.22}$	–	396.9/660	1.20/2.28	<4.0
J173527.5–325554	$7.5^{+3.0}_{-2.5}$	$0.54^{+0.60}_{-0.55}$	$13.1^{+2.5}_{-2.0}$	$0.55^{+0.30}_{-0.40}$	541.0/659	1.18/2.28	<11
J174026.8–365537	$0.1^{+0.4}_{-0.1}$	$-0.30^{+0.30}_{-0.24}$	$7.2^{+1.3}_{-1.1}$	–	507.7/660	0.42/0.11	<0.5
J174437.3–323222[h]	$2.4^{+0.8}_{-0.6}$	$0.97^{+0.34}_{-0.32}$	3.5 ± 0.4	–	526.0/660	0.67/0.47	0.2–3.2
J175039.4–264436	$13.4^{+7.8}_{-5.5}$	$0.44^{+0.84}_{-0.72}$	$4.5^{+1.9}_{-0.7}$	–	469.2/660	1.16/4.66	<21
J175834.5–212321	$15.6^{+6.0}_{-5.0}$	$0.23^{+0.59}_{-0.54}$	$11.4^{+2.3}_{-1.4}$	–	516.0/660	0.76/0.48	9–22
J181328.0–163548	$11.0^{+5.6}_{-4.1}$	$1.44^{+0.89}_{-0.79}$	$3.0^{+5.0}_{-2.1}$	–	363.6/660	1.14/0.80	4–17
J181722.1–250842	$0.11^{+0.35}_{-0.11}$	$-0.28^{+0.19}_{-0.28}$	$8.5^{+2.3}_{-1.1}$	$1.0^{+0.0}_{-0.8}$	607.0/659	0.23/0.00	<0.46
J183049.9–123219	$0.40^{+0.29}_{-0.25}$	$0.54^{+0.18}_{-0.31}$	$9.5^{+3.2}_{-1.4}$	$0.88^{+0.12}_{-0.48}$	588.7/659	1.02/0.66	<0.69
J184825.4–004635	68^{+28}_{-23}	$3.0^{+1.9}_{-1.6}$	$124^{+11,949}_{-116}$	–	298.1/660	1.83/1.14	41–96
J192626.9+132205	$0.31^{+0.13}_{-0.12}$	0.75 ± 0.12	$9.1^{+0.6}_{-0.5}$	–	647.2/660	0.95/0.37	<0.44
J194356.2+211823	$1.89^{+0.25}_{-0.22}$	1.83 ± 0.11	29^{+24}_{-5}	$0.68^{+0.32}_{-0.18}$	693.5/658	0.84/0.054	0.7–2.1

[a]The parameters are for power-law fits to the *Chandra*/ACIS spectra and include photoelectric absorption with cross sections from Balucinska-Church & McCammon (1992) and abundances from Wilms, Allen & McCray (2000). In general, the measured value of $N_{\rm H}$ and the errors on $N_{\rm H}$ are scaled-down by ∼30% if solar abundances (Anders & Grevesse 1989) rather than the approximation to average interstellar abundances (Wilms, Allen & McCray 2000). A pile-up correction was applied in the cases where pile-up parameters are given. The PSF fraction (Davis 2001) was left fixed to 0.95 (the default value) except for the CXOU J194356.2+211823 spectrum, where it was left as a free parameter. In this case, the PSF fraction dropped to $0.35^{+0.26}_{-0.13}$, presumably because this is a bright source that is relatively far (4.9 arcminutes) off-axis. We performed fits without re-binning the data and using Cash statistics. Errors in this table are at the 90% confidence level ($\Delta C = 2.7$).

[b]Unabsorbed 0.3–10 keV flux in units of 10^{-12} erg cm^{-2} s^{-1}.

[c]The grade migration parameter in the pile-up model (Davis 2001). The probability that n events will be piled together but will still be retained after data filtering is α^{n-1}.

[d]The Cash statistic and degrees of freedom for the best fit model.

[e]The atomic hydrogen column density through the Galaxy from Kalberla et al. (2005). We also give the molecular hydrogen column density through the Galaxy, using a CO map and conversion to $N_{\rm H_2}$ (Dame, Hartmann & Thaddeus 2001).

[f]The estimate for the column density due to material local to the source (see text for details on how the limits are derived). An upper limit indicates no evidence for local absorption (although it also cannot be ruled out in any case), and a range indicates evidence for slight or significant local absorption.

[g]A strong iron line is present and is included in the model as a Gaussian. The parameters are $E_{\rm line} = 6.70^{+0.25}_{-0.17}$ keV, $\sigma_{\rm line} = 0.27^{+0.21}_{-0.14}$ keV, and $N_{\rm line} = (7.0^{+4.8}_{-3.4}) \times 10^{-5}$ photons cm^{-2} s^{-1}, with an equivalent width of 945 eV.

[h]This is the spectrum of the point source a few arcminutes from the center of the nebula.

TABLE 4
QUANTITIES FOR CALCULATING THE PROBABILITY OF SPURIOUS ASSOCIATIONS

CXOU Name	$F_{\rm 2-10\ keV}$[a]	$N(>F_{\rm 2-10\ keV})$ (deg^{-2})[b]	θ (arcmin)[c]	$\theta_{INTEGRAL}$ (arcmin)[d]	Probability (%)
J110926.4–650224	3.3×10^{-12}	0.59	6.02	5.5	1.9
J131825.0–625815	2.6×10^{-13}	4.32	1.94	3.8	5.4
J143308.3–611539	6.3×10^{-12}	0.35	4.02	3.9	0.49
J144628.2–641624	4.5×10^{-12}	0.46	1.46	3.7	0.55
J155246.9–502953	1.6×10^{-12}	1.05	1.59	3.9	1.4
J162826.8–502239	6.7×10^{-12}	0.33	3.12	4.4	0.56
J173518.7–325428	1.1×10^{-12}	1.35	1.83	2.2	0.57
J173527.5–325554	9.7×10^{-12}	0.25	1.34	2.2	0.11
J174026.8–365537	7.0×10^{-12}	0.32	0.84	3.5	0.34
J174437.3–323222	2.7×10^{-12}	0.68	3.77	2.2	0.84
J175039.4–264436	3.0×10^{-12}	0.62	2.97	2.6	0.48
J175834.5–212321	7.7×10^{-12}	0.30	3.81	3.3	0.38
J181328.0–163548	1.4×10^{-12}	1.16	0.97	3.8	1.5
J181722.1–250842	8.4×10^{-12}	0.28	0.86	2.2	0.12
J183049.9–123219	8.6×10^{-12}	0.27	0.83	3.3	0.26
J184825.4–004635	1.8×10^{-12}	0.96	0.55	3.4	0.97
J192626.9+132205	7.9×10^{-12}	0.29	4.79	3.7	0.58
J194356.2+211823	1.4×10^{-11}	0.19	4.88	4.9	0.39

[a]The absorbed 2–10 keV flux in units of ergs cm^{-2} s^{-1}.

[b]The X-ray source density at the 2–10 keV flux level for each source from the *ASCA* survey of the Galactic plane (Sugizaki et al. 2001).

[c]The angular distance between the center of the *INTEGRAL* error circle and the source.

[d]The 90% confidence *INTEGRAL* error radius (Bird et al. 2006).

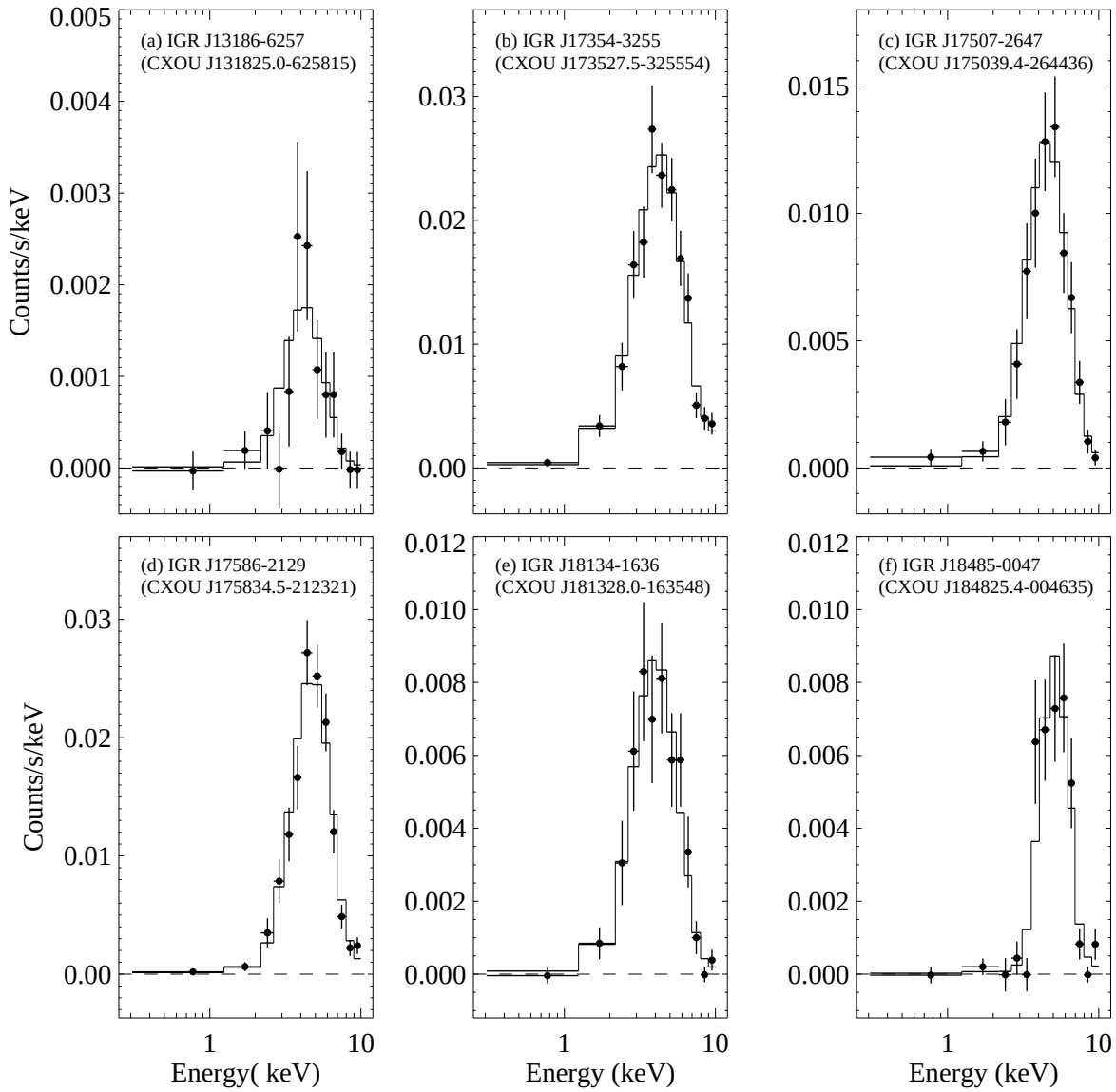

FIG. 3.— *Chandra* ACIS-I spectra for the six sources that show the highest column density measurements. IGR J13186–6257 *(a)*, IGR J17586–2129 *(d)*, IGR J18134–1636 *(e)*, and IGR J18485–0047 *(f)* require levels of $N_{\rm H}$ in excess of the Galactic levels (see Table 3) while IGR J17354–3255 *(b)* and IGR J17507–2647 *(c)* may or may not be locally absorbed.

4. DISCUSSION

4.1. *Extended Sources*

4.1.1. *IGR J14003–6326*

IGR J14003–6326 was discovered by *INTEGRAL* in 2006 (Keek, Kuiper & Hermsen 2006). Although it was observed by *Swift*, no conclusion was reached on its nature (Malizia et al. 2007). Figure 4 shows 0.3–10 keV *Chandra*/ACIS images of the IGR J14003–6326 field. The widest view (Figure 4a) shows the presence of a nearly circular source with a radius of 1′.5, and this is the only bright source detected in the 3′.9 radius *INTEGRAL* error circle. The position and the fact that it is a hard source make it essentially certain that this is the IGR source, and the morphology and hardness allow us to identify this source as a supernova remnant (SNR). For Figure 4b, we zoom-in toward the center of the SNR to show that there is significant structure near the center at size scales of tens of arcseconds. We suspect that this is a pulsar wind nebula (PWN). Finally, Figure 4c shows the *Chandra* image without any pixel binning, and it is clear that there is a point-like source near the center of the SNR where a putative neutron star might reside. The number of counts in the brightest pixel is 82, and the central 9 pixels have 298 counts. The position of this point-like source is R.A. (J2000) = $14^{\rm h}00^{\rm m}45^{\rm s}.69$, Decl. (J2000) = –63°25′42″.6, and it is very close to the center of the SNR. Despite the relative brightness of the point-like source, this is only a small fraction of the 4075 counts collected for the entire SNR. Thus, the emission detected by *INTEGRAL* likely comes from the PWN or the SNR.

We have used the CIAO routine `specextract` to produce a spectrum from a circular region centered on the point-like source with a radius of 1′.5, while the background is taken from a source-free rectangular region on the same ACIS-I chip. The 0.3–10 keV energy spectrum is well-described by an absorbed power-law, with this model giving χ^2_ν = 0.92 for 161 dof. The measured $N_{\rm H}$ is $(3.1 \pm 0.3) \times 10^{22}$ cm^{-2}, which is somewhat higher than the Galactic value ($N_{\rm H} + 2N_{\rm H_2}$) of 2.1×10^{22} cm^{-2}. The measured power-law photon index is $\Gamma = 1.83 \pm 0.13$, and the unabsorbed 0.3–10 keV flux is 3.6×10^{-11} ergs cm^{-2} s^{-1}. The unabsorbed 2–10 keV flux is 1.9×10^{-11} ergs cm^{-2} s^{-1}, which corresponds to ∼1 millicrab.

There has only been one other IGR source identified as a SNR, IGR J18135–1751, and it has been identified as the TeV source HESS J1813-178 (Ubertini et al. 2005). Searches of the *High Energy Stereoscopic System (HESS)* source catalog[7] as well as the SIMBAD database and the *Fermi* Large Area Bright Gamma-Ray Source List (Abdo 2009) do not indicate that IGR J14003–6326 is identified with any TeV or GeV source. The 20–100 keV flux for IGR J14003–6326 is 1.8×10^{-11} ergs cm^{-2} s^{-1} (Bird et al. 2006), which is only slightly less than the 3×10^{-11} ergs cm^{-2} s^{-1} flux of IGR J18135–1751 (Ubertini et al. 2005). However, Ubertini et al. (2005) show that the TeV emission for IGR J18135–1751 is more than an order of magnitude in excess of an extrapolation of the X-ray power-law, and Helfand et al. (2007) point out that the TeV-to-X-ray luminosity ratio for IGR J18135–1751 is extreme with a value close to unity, which is much higher than the ratio of 0.06 measured for the Crab Nebula and also significantly higher than the highest ratios known for PWNe (e.g., 0.5 for PSR 1509–58 and 0.3 for Vela X). It has been suggested that the possible proximity to the star forming region W33 to IGR J18135–1751 may provide a higher density of seed photons for Inverse Compton scattering to TeV energies (Funk et al. 2007; Helfand et al. 2007). Thus, the non-detection of TeV emission from IGR J14003–6326 is not surprising and suggests that its high energy properties are more similar to the previously known PWN than to IGR J18135–1751.

[7] See http://www.mpi-hd.mpg.de/hfm/HESS/pages/home/sources.

4.1.2. *IGR J17448–3232*

From a *Swift* observation, Landi et al. (2007b) mentioned the presence of diffuse emission in the IGR J17448–3232 field, and our *Chandra* observation confirms this. Figure 5a shows a rebinned 0.3–10 keV image along with the 2′.2 radius *INTEGRAL* error circle, which is centered on the extended source. Like the previous source, the extended source associated with IGR J17448–3232 is a nearly circular, and is likely a SNR. However, we do not see any evidence for a PWN within the SNR, and the only point-like source is CXOU J174437.3–323222, which is a hard source at the edge of the SNR (see Figure 5b). We extracted a *Chandra* spectrum from the extended source, using a circular extraction region with a radius of 3′. The spectrum is well-described (χ^2_ν = 0.99 for 163 dof) by an absorbed power-law with $N_{\rm H} = (2.5^{+0.5}_{-0.4}) \times 10^{22}$ cm^{-2}, which is somewhat above the interstellar column density ($N_{\rm H} + 2N_{\rm H_2}$) of 1.6×10^{22} cm^{-2}. The power-law photon index is $\Gamma = 1.27^{+0.22}_{-0.21}$, and the 0.3–10 keV unabsorbed flux is 2.3×10^{-11} ergs cm^{-2} s^{-1}. We do not find any high-energy counterparts to this SNR in the *HESS* or *Fermi* catalogs. As discussed above, even though TeV emission is detected for IGR J18135–1751, the non-detection of TeV emission for IGR J17448–3232 is not surprising because IGR J18135–1751 is an extreme case. In addition, IGR J17448–3232 may be even less likely to emit strong TeV emission because we do not see a PWN within the SNR.

The fact that the position at the center of the extended source agrees well with the *INTEGRAL* position argues that the SNR is primarily producing the 1.1×10^{-11} ergs cm^{-2} s^{-1} flux that *INTEGRAL* is detecting in the 20–100 keV band (Bird et al. 2006). However, it is still possible that the hard point source, CXOU J174437.3–323222, is associated with the SNR. The hard point source does not have counterparts in the 2MASS, DENIS, USNO-B1.0, or USNO-A2.0 catalogs; however, the K_s-band image shown in Figure 5c shows that the *Chandra* position is on the edge of the point spread function of a relatively bright IR source, so better optical/IR images are necessary. If CXOU J174437.3–323222 is an isolated neutron star that received a kick when the supernova occurred, it should be very faint in the optical and IR. While the association between the SNR and CXOU J174437.3–323222 is intriguing, further work is necessary for confirmation.

4.2. *Point Sources*

IGR J11098–6457: Based on an earlier *Swift* observation, two possible counterparts were considered, and it was found that 1RXS J110927.4–650245 is the more likely counterpart due to its hard X-ray spectrum (Landi et al. 2008b). The position of CXOU J110926.4–650224, the source that we find to be the most likely counterpart, is consistent with the *Swift* position. There are no 2MASS, DENIS, USNO-B1.0, or USNO-A2.0 sources consistent with the *Chandra* position. However, the 2MASS K_s-band image shown in Figure 6a shows that there appears to be a faint IR source at the *Chandra* position.

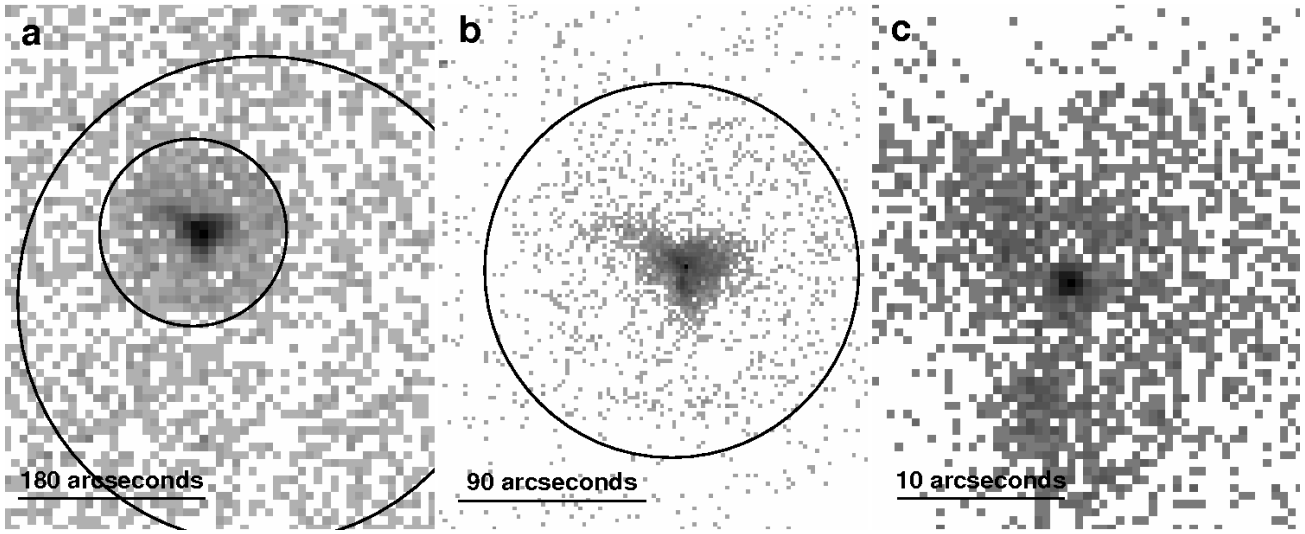

FIG. 4.— *Chandra* 0.3–10 keV images for IGR J14003–6326. *(a)* The pixel size in this image is 7″.9. The larger circle shows the 90% confidence *INTEGRAL* error circle, which has a radius of 3′.9. The smaller circle has a radius of 1′.5, and marks the approximate extent of the supernova remnant (SNR). *(b)* The pixel size in this image is 1″.97, and the image is meant to highlight the putative pulsar wind nebula. The 1′.5 radius circle is shown. *(c)* The pixel size in this unbinned image is 0″.492, and the image is meant to highlight the point-like source near the center of the SNR. In all 3 images, North is up and East is to the left.

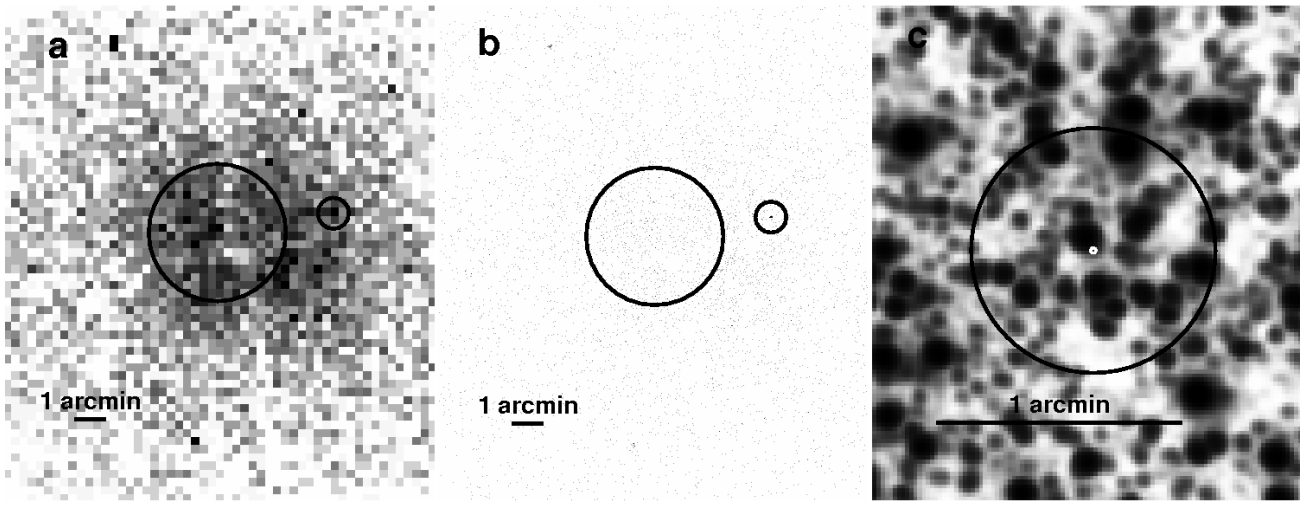

FIG. 5.— Images of the IGR J17448–3232 field. *(a)* A *Chandra* 0.3–10 keV image rebinned to a pixel size of 15″.7. The larger circle shows the 90% confidence *INTEGRAL* error circle, which has a radius of 2′.2. The smaller circle has a radius of 0′.5, and marks the location of the hard point source, CXOU J174437.3–323222. The extended source is likely a supernova remnant (SNR), and we suggest that the hard point source may be an associated pulsar. *(b)* The pixel size in this image is 0″.98. The same two circles are plotted, and the image is meant to highlight the hard point source. *(c)* A 2MASS K_s-band image of the region near the hard point source. The black circle is the same 0′.5-radius circle shown in the other two panels, and the *Chandra* 90% confidence error circle is shown in white. In all 3 images, North is up and East is to the left.

The *Chandra* energy spectrum is consistent with a power-law with a photon index of $\Gamma = 1.43 \pm 0.17$ and a column density consistent with the Galactic column density (see Table 3). The 2–10 keV absorbed flux is 3.3×10^{-12} ergs cm^{-2} s^{-1}. Thus, the spectrum measured by *Chandra* is consistent with that measured by *Swift*, which found $\Gamma \sim 1.2$ and a 2–10 keV flux of 2.7×10^{-12} ergs cm^{-2} s^{-1} (Landi et al. 2008b).

IGR J13186–6257: The position of CXOU J131825.0–625815 is consistent with the *Swift* position for this IGR source reported in Landi et al. (2008c). The refined *Chandra* position allows us to identify the IR counterpart as 2MASS J13182505–6258156, which is 0″.2 from the *Chandra* position and has IR magnitudes of J = 13.58, H = 12.69, K_s = 12.84 ± 0.05 (see Table 5 and Figure 7a). There are no corresponding sources in the DENIS, USNO-B1.0, or USNO-A2.0 catalogs. Although Landi et al. (2008c) report that the *Swift* spectrum of this source is unabsorbed, we measure $N_{\rm H} = (1.8^{+6.6}_{-1.3}) \times 10^{23}$ cm^{-2}, and we find that $N_{\rm H,local}$ is in the range $(2\text{–}84) \times 10^{22}$ cm^{-2} (see Table 3). While we cannot make a definitive statement about the nature of the source, high and variable column densities have been seen for several of the IGR HMXBs.

IGR J14331–6112: A *Swift* position was previously obtained for this source (Landi et al. 2007a), leading to a likely identification with a USNO-B1.0 source. Follow-up optical spectroscopy indicated a HMXB harboring an optical com-

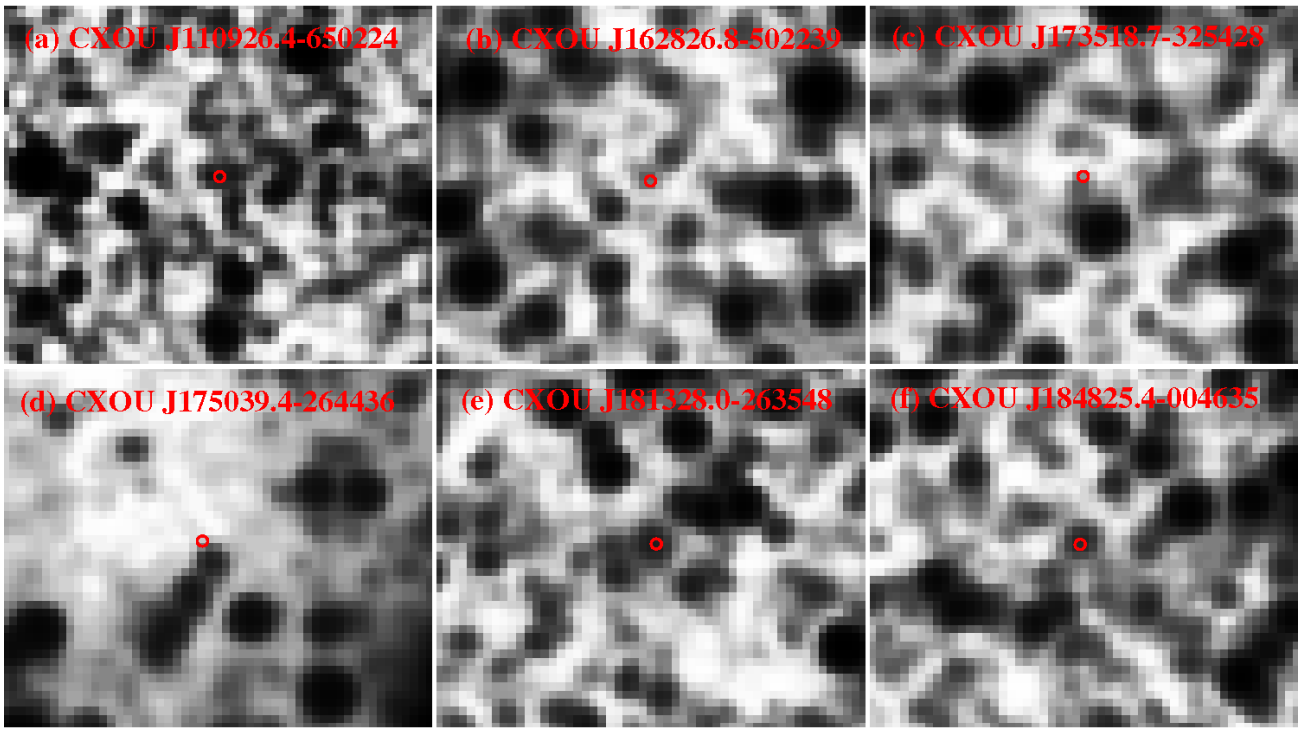

FIG. 6.— 2MASS K_s-band images with *Chandra* 90% confidence error circles for 6 IGR sources for which there are no counterparts in the 2MASS, DENIS, USNO-B1.0, or USNO-A2.0 catalogs. However, some of the images, *(a)*, *(b)*, *(e)*, and *(f)* suggest that there are faint IR counterparts. The images are for the following sources: *(a)* CXOU J110926.4–650224, *(b)* CXOU J162826.8–502239, *(c)* CXOU J173518.7–325428, *(d)* CXOU J175039.4–264436, *(e)* CXOU J181328.0–263548, and *(f)* CXOU J184825.4–004635. In each image, the pixel size is 1″ and North is up and East is to the left. The images are 52″ in the East-West direction and 43″ in the North-South direction.

panion with a B III or B V spectral type (Masetti et al. 2008). The position of CXOU J143308.3–611539 is consistent with the HMXB, confirming the identification. The *Chandra* energy spectrum is consistent with a power-law with a photon index of $\Gamma = 0.34^{+0.37}_{-0.33}$, which is similar to the value of $\Gamma \sim 0.7$ quoted for the *Swift* spectrum. However, a new result from the *Chandra* spectrum is the discovery of a very strong iron Kα emission line with an equivalent width of ∼945 eV. Strong iron lines have been seen for some of the other IGR HMXBs (Matt & Guainazzi 2003; Walter et al. 2003, 2006), but they are usually associated with the class of obscured HMXBs. Although we measure a relatively low column density of $N_{\rm H} = (2.2^{+0.9}_{-0.8}) \times 10^{22}$ cm^{-2}, consistent with the Galactic value, for CXOU J143308.3–611539, it should be noted that the presence of a soft excess can cause artificially low column densities to be measured in spectra with lower statistical quality (Tomsick et al. 2009). For the *Chandra* spectrum, if we add a second power-law component to account for a putative soft excess (as in Tomsick et al. 2009), the find that the column density for the primary power-law component can be as high as 1.1×10^{23} cm^{-2}.

IGR J14471–6414: A *Swift* position was previously obtained for this source (Landi et al. 2007a), and follow-up optical spectroscopy indicated the presence of a Seyfert 1.2 AGN with a redshift of $z = 0.053$ in the *Swift* error circle (Masetti et al. 2008). The position of CXOU J144628.2–641624 is consistent with the position of the AGN, confirming the association.

IGR J15529–5029: The position of CXOU J155246.9–502953 is consistent with the *Swift* position for this IGR source reported in Landi et al. (2008c). The refined *Chandra* position allows us to identify the IR counterpart as 2MASS J15524694–5029534, which is 0″.2 from the *Chandra* position and has IR magnitudes of $J = 15.84 \pm 0.10$, $H = 15.27 \pm 0.13$, and $K_s = 14.77 \pm 0.12$. In addition, USNO-B1.0 0395-0509024 and USNO-A2.0 0375-25891641 are 0″.3 from the *Chandra* position, and the optical magnitudes are listed as $R = 18.6$ and $B = 21.4$ for the former and $R = 17.6$ and $B = 20.3$ for the latter (see Table 5). Although we cannot conclude definitively on the nature of this source, the X-ray spectrum measured by *Swift* (a power-law with $\Gamma \sim 0.9$) and *Chandra* (a power-law with $\Gamma = 0.60^{+0.30}_{-0.28}$) are harder than would be expected for an AGN (Malizia et al. 2007), and we suggest that a CV or X-ray binary nature is more likely.

IGR J16287–5021: The *Chandra* information for CXOU J162826.8–502239 was reported previously in Tomsick et al. (2008c), and the *Chandra* and *Swift* results for this source are discussed in detail in Rodriguez, Tomsick & Chaty (2009). Both *Chandra* and *Swift* detect the source at about the same flux level and with a low level of absorption. However, the *Chandra* power-law index of $\Gamma = -0.82^{+0.32}_{-0.26}$ is significantly harder than the value of $\Gamma = 0.9 \pm 0.8$ found by *Swift*. There are no 2MASS, DENIS, USNO-B1.0, or USNO-A2.0 sources consistent with the *Chandra* position. However, Figure 6b shows the 2MASS K_s-band image for this field, and there is a faint IR source that appears to be consistent with the *Chandra* position. The very hard X-ray spectrum suggests a CV or X-ray binary nature rather than an AGN nature, and perhaps the lack of an optical counterpart along with the faint IR candidate counterpart favors a relatively distant X-ray binary (likely an HMXB) rather than a CV.

IGR J17354–3255: This source was discovered within

$\sim$5° of the Galactic center by *INTEGRAL* in 2006 (Kuulkers et al. 2006; Bird et al. 2006). There are two relatively bright and hard *Chandra* sources within the *INTEGRAL* error circle (see also Tomsick 2009), and these were also detected during a *Swift* observation made in 2009 April (Vercellone et al. 2009). The position of CXOU J173527.5–325554, the brighter and harder of the two sources, is within 0″.2 of 2MASS J17352760–3255544, which has $J = 12.51 \pm 0.05$, $H = 10.99 \pm 0.04$, and $K_s = 10.27 \pm 0.03$. The source also appears in the DENIS catalog with similar J and K_s magnitudes (see Table 5). However, it must be quite faint optically since it is not detected in the DENIS I-band, and it does not appear in the USNO catalogs. The large $J-K_s$ value, high inferred optical extinction, and the relatively high X-ray column density $(7.5^{+3.0}_{-2.5}) \times 10^{22}$ cm^{-2} argue that the source is distant, probably either an X-ray binary near the Galactic center or an AGN. However, as argued above, the hard power-law index of $\Gamma = 0.54^{+0.60}_{-0.55}$ argues against the AGN possibility and for the possibility that the source is an HMXB. The other *Chandra* source, CXOU J173518.7–325428, does not have 2MASS, DENIS, USNO-B1.0, or USNO-A2.0 counterparts. Although the K_s-band image (see Figure 6c) shows a faint IR source within a couple arcseconds, it is not close enough to be associated with the *Chandra* source. It is possible that both *Chandra* sources contribute to the flux detected by *INTEGRAL*, but CXOU J173527.5–325554 would probably be a more interesting source for any further follow-up work. Another reason for interest in pursuing the nature of IGR J17354–3255 is that its position is consistent with the position of the gamma-ray transient AGL J1734–3310 (Bulgarelli et al. 2009).

IGR J17404–3655: A *Swift* position was previously obtained for this source (Landi et al. 2008c), leading to a likely identification with a USNO-B1.0 source. From follow-up optical spectroscopy that showed a strong Hα emission line but no other strong emission or absorption line features, Masetti et al. (2009) identify the source as an X-ray binary. The position of CXOU J174026.8–365537 is consistent with the X-ray binary, confirming the identification. However, we are dubious about the further classification of the source as an LMXB rather than an HMXB. The *Swift* spectrum showed a power-law index of $\Gamma \sim 0.24$ (Landi et al. 2008c), and *Chandra* shows an even harder spectrum with $\Gamma = -0.30^{+0.30}_{-0.24}$, which would be very unusual for typical LMXBs and is more commonly seen for HMXBs that harbor more highly magnetized neutron stars.

IGR J17507–2647: This source was discovered within $\sim$2.5° of the Galactic center by *INTEGRAL* (Bird et al. 2006), but no further information about this source has been reported until now. The *Chandra* energy spectrum for CXOU J175039.4–264436 exhibits a high column density with $N_{\rm H} = (1.34^{+0.78}_{-0.55}) \times 10^{23}$ cm^{-2}. Although this may indicate that the source is obscured (e.g., an obscured HMXB), Table 3 indicates that $N_{\rm H_2}$ is very high along this line-of-sight, 4.7×10^{22} cm^{-2}, and the upper limit on $N_{\rm H,local}$ indicates that the measured absorption may be interstellar. CXOU J175039.4–264436 does not have 2MASS, DENIS, USNO-B1.0, or USNO-A2.0 counterparts (also see Figure 6d), providing further evidence that the absorption is interstellar. Although we cannot say definitively what the nature of the source is, the result that there is a high level of interstellar absorption also indicates that the source is distant, possibly close to the Galactic center region at $\sim$8.5 kpc. This would argue for a luminosity of $\sim 4 \times 10^{34}$ ergs s^{-1}, which would suggest that the source is an X-ray binary rather than a CV.

IGR J17586–2129: This source was discovered by *INTEGRAL* (Bird et al. 2006), but no further information about this source has been reported until now. As shown in Table 3, CXOU J175834.5–212321 has $N_{\rm H,local}$ in the range $(9–22) \times 10^{22}$ cm^{-2}, providing excellent evidence that this source has local absorption. The position of the *Chandra* source is within 0″.1 of 2MASS J17583455–2123215, which has IR magnitudes of $J = 11.38 \pm 0.04$, $H = 9.53 \pm 0.03$, and $K_s = 8.44 \pm 0.03$, and it is within 0″.3 of DENIS J175834.5-212321, which has similar IR magnitudes and an I-band magnitude of 15.26 ± 0.05 (see Table 5). The source is not present in the USNO catalogs. The magnitudes clearly indicate a highly reddened source, suggesting a large distance (likely at least several kpc). The 0.3–10 keV flux (see Table 3) indicates a luminosity of 3×10^{34} ergs s^{-1} for a fiducial distance of 5 kpc, which is too bright for the source to be a CV. Also, the hard X-ray spectrum, $\Gamma = 0.23^{+0.59}_{-0.54}$, suggests an HMXB rather than an AGN. Overall, this source is an excellent candidate for being one of the obscured IGR HMXBs.

IGR J18134–1636: This source was discovered by *INTEGRAL* (Bird et al. 2006), but no further information about this source has been reported until now. The *Chandra* spectrum for CXOU J181328.0–163548 shows evidence for local absorption with $N_{\rm H,local}$ in the range $(4–17) \times 10^{22}$ cm^{-2}. There are no convincing optical or IR counterparts to the *Chandra* source in the 2MASS, DENIS, or USNO catalogs. The nearest source in these 4 catalogs is a USNO-B1.0 source that is 1″.24 away from CXOU J181328.0–163548; however, this is too far away to claim an association. The IR source shown in Figure 6e that appears to be consistent with the *Chandra* position is not listed in the 2MASS catalog, and this may be the IR counterpart. The high column density makes it unlikely that this source is a CV. However, with a power-law index of $\Gamma = 1.4^{+0.9}_{-0.8}$, it could either be an X-ray binary or an AGN.

IGR J18173–2509: The position of CXOU J181722.1–250842 is consistent with the *Swift* position for this IGR source reported in Landi et al. (2008a). An optical source in the *Swift* error circle was followed-up with optical spectroscopy, showing that the source is a CV at a distance of $\sim$330 pc (Masetti et al. 2009). The 0.3–10 keV flux from the *Chandra* spectrum of 8.5×10^{-12} ergs cm^{-2} s^{-1} is similar to the 2–10 keV value quoted for the *Swift* spectrum of 1.3×10^{-11} ergs cm^{-2} s^{-1}. At a distance of 330 pc, this flux corresponds to a luminosity of $\sim 10^{32}$ ergs s^{-1}, typical of CVs. However, we find that the *Chandra* spectrum is well-described by a single power-law in contrast to the two power-law model described for the *Swift* spectrum by Landi et al. (2008a).

IGR J18308–1232: This source was previously identified with the *XMM-Newton* slew source XMMLS1 J183049.6–123218 (Ibarra, Kuulkers & Saxton 2008), and the positions of CXOU J183049.9–123219 and the *XMM-Newton* source are consistent. Follow-up optical spectroscopy has already been obtained for the correct optical counterpart, USNO-B1.0 0774-0551687, indicating that the source is a CV (Parisi et al. 2008; Masetti et al. 2009; Butler et al. 2009). The *Chandra* flux level and energy spectrum are significantly different from the *XMM-Newton* measurements. The unabsorbed 0.3–10 keV *Chandra* flux level is about 4 times higher than reported in Ibarra, Kuulkers & Saxton (2008) for *XMM-Newton*. Also, the *Chandra* photon index is $\Gamma = 0.54^{+0.18}_{-0.31}$, which is significantly harder than the value of $\Gamma = 1.7$ reported for *XMM-*

TABLE 5
NEW OPTICAL/INFRARED IDENTIFICATIONS

Catalog/Source[a]	Separation	Magnitudes		
IGR J13186–6257/CXOU J131825.0–625815				
2MASS J13182505–6258156	0″.2	$J = 13.58$	$H = 12.69$	$K_s = 12.84 \pm 0.05$
IGR J15529–5029/CXOU J155246.9–502953				
2MASS J15524694–5029534	0″.2	$J = 15.84 \pm 0.10$	$H = 15.27 \pm 0.13$	$K_s = 14.77 \pm 0.12$
USNO-B1.0 0395-0509024	0″.3	$B = 21.4 \pm 0.3$	$R = 18.6 \pm 0.3$	—
USNO-A2.0 0375-25891641	0″.3	$B = 20.3 \pm 0.5$	$R = 17.6 \pm 0.4$	—
IGR J17354–3255/CXOU J173527.5–325554				
2MASS J17352760–3255544	0″.2	$J = 12.51 \pm 0.05$	$H = 10.99 \pm 0.04$	$K_s = 10.27 \pm 0.03$
DENIS J173527.6–325554	0″.2	$J = 12.36 \pm 0.07$	—	$K_s = 10.12 \pm 0.06$
IGR J17586–2129/CXOU J175834.5–212321				
2MASS J17583455–2123215	0″.1	$J = 11.38 \pm 0.04$	$H = 9.53 \pm 0.03$	$K_s = 8.44 \pm 0.03$
DENIS J175834.5–212321	0″.3	$I = 15.26 \pm 0.05$	$J = 11.25 \pm 0.06$	$K_s = 8.38 \pm 0.05$

[a]The catalogs are the 2 Micron All-Sky Survey (2MASS), the Deep Near Infrared Survey of the Southern Sky (DENIS), and the United States Naval Observatory (USNO-B1.0 and USNO-A2.0). The 2MASS K_s-band images for these four sources are shown in Figure 7

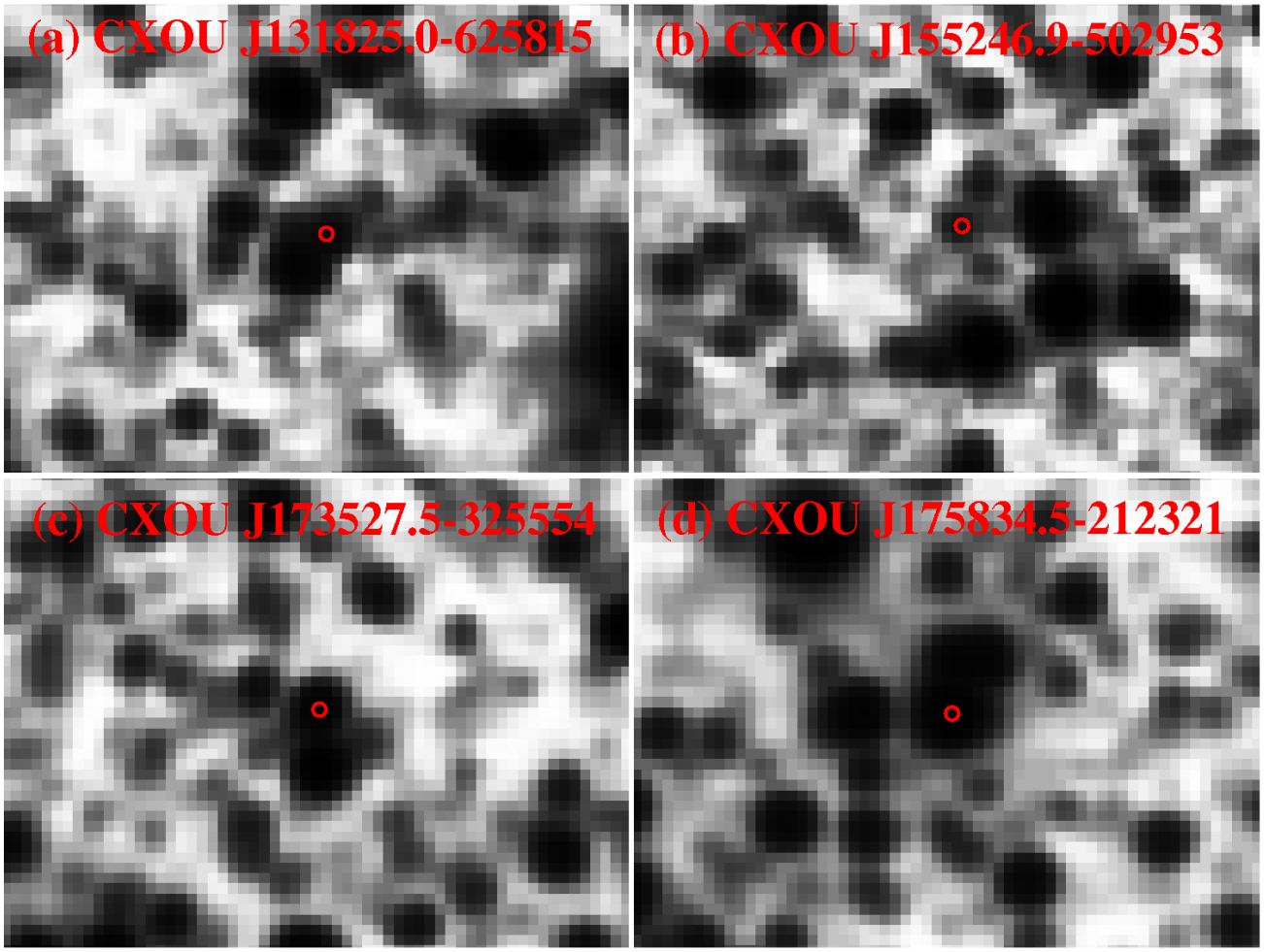

FIG. 7.— 2MASS K_s-band images with *Chandra* 90% confidence error circles for the 4 IGR sources with new optical/IR identifications (see Table 5). The images are for the following sources: *(a)* CXOU J131825.0–625815, *(b)* CXOU J155246.9–502953, *(c)* CXOU J173527.5–325554, and *(d)* CXOU J175834.5–212321. In each image, the pixel size is 1″ and North is up and East is to the left. The images are 60″ in the East-West direction and 45″ in the North-South direction.

Newton. At the estimated distance to the source of 200–300 pc (Masetti et al. 2009; Butler et al. 2009), the *Chandra* flux level corresponds to an X-ray luminosity of $\sim 10^{32}$ ergs s^{-1}, which is typical for CVs.

IGR J18485–0047: The position of CXOU J184825.4–004635 is consistent with the *Swift* position for this IGR source reported in Landi et al. (2007c). The *Chandra* position does not correspond to any cataloged 2MASS, DE-

NIS, USNO-B1.0, or USNO-A2.0 sources, but the K_s-band image shown in Figure 6f suggests that a faint IR source may be associated with CXOU J184825.4–004635. Also, Landi et al. (2007c) noted a possible association between IGR J18485–0047 and the radio source GPSR5 31.897+0.317 (Becker et al. 1994). The *Chandra* source is within $1''.1$ of the radio source, and the 90% confidence error radius on the radio source is $2''.2$, so the association is likely. The flux of the radio source is 8.9 mJy at 5 GHz and 21 mJy at 1.4 GHz, and it is consistent with being a point source. As for the X-ray properties, both the *Swift* and *Chandra* spectra show evidence for absorption well in excess of the Galactic value. The association with a radio source may indicate an AGN nature for the source; however, CVs and X-ray binaries can also be radio emitters, so the classification is not certain. If the source is an AGN, then the high levels of absorption would indicate a Seyfert 2 classification.

IGR J19267+1325: The *Chandra* information for CXOU J192626.9+132205 was reported previously in Tomsick et al. (2008c), and the *Chandra* and *Swift* results for this source are discussed in detail in Rodriguez, Tomsick & Chaty (2009). After the identification of the optical counterpart (Tomsick et al. 2008c), follow-up optical spectroscopy showed that the source is a CV (Steeghs et al. 2008; Masetti et al. 2009; Butler et al. 2009). Furthermore, an X-ray period of 938.6 s has been measured and is identified as the white dwarf spin period, indicating that the source is a CV of Intermediate Polar type (Evans, Beardmore & Osborne 2008). A second period may also be present at 4.58 hours, and this may be the binary orbital period (Evans, Beardmore & Osborne 2008). Somewhat discrepant distances of 580 pc (Masetti et al. 2009) and 250 pc (Butler et al. 2009) have been derived. For this range of distances, the X-ray flux that we measure indicates a range of 0.3–10 keV luminosities of 7×10^{31} to 4×10^{32} ergs s^{-1}.

IGR J19443+2117: Based on a *Swift* detection of this source, Landi et al. (2009) suggest associations with the radio source NVSS J194356+211826 and the IR source 2MASS J19435624+2118233. We confirm these associations as CXOU J194356.2+211823 is within $0''.3$ of the 2MASS source. Landi et al. (2009) discuss the nature of the source, which is a relatively bright radio source (103 mJy at 1.4 GHz) and also has a K_s-magnitude of 13.98 ± 0.07. The *Chandra* spectrum and flux are similar to those reported by Landi et al. (2009), but we find even stronger evidence that the column density is in excess of the Galactic value. Overall, we agree with the conclusion of Landi et al. (2009) that IGR J19443+2117 is most likely an AGN, but an optical or IR spectral confirmation would strengthen this conclusion.

5. SUMMARY AND CONCLUSIONS

The main goal of this *Chandra* project has been to localize and measure the soft X-ray spectra of IGR sources in the Galactic plane in order to determine their nature or to guide follow-up observations to determine their nature. In this paper, we have reported results from 22 *Chandra* observations, and we have identified likely soft X-ray counterparts in 18 cases. Here, we summarize the different types of sources that we have found.

Two X-ray binaries and five X-ray binary candidates: We confirm that IGR J14331–6112 is an HMXB based on its positional coincidence with the previously suggested counterpart (Masetti et al. 2008), and we show that this source has a very strong iron Kα emission line, which is similar to what has been seen for some of the other IGR HMXBs. We also confirm the Masetti et al. (2009) optical identification of IGR J17404–3655. While we agree that the source is an X-ray binary, we argue that the hard X-ray spectrum may indicate that the source is an HMXB rather than an LMXB. Hard X-ray spectra ($\Gamma < 1$) combined with large optical/IR extinctions (and thus, large distances) argue for an HMXB nature, and we suggest that IGR J16287–5021, IGR J17354–3255, IGR J17507–2647, and IGR J17586–2129 may be HMXBs based on this evidence. Finally, comparing *Swift* and *Chandra* spectra shows that the column density for IGR J13186–6257 is high and variable, which suggests the possibility that the source is and HMXB.

Three CVs and one CV candidate: For IGR J19267+1325, the *Chandra* position led to the identification of the optical counterpart that was shown to be a CV. In addition, we confirm the previously suggested optical identifications for IGR J18173–2509 and IGR J18308–1232, and these are also CVs. We also mention the new possibility that IGR J15529–5029 may be a CV based on a hard X-ray spectrum ($\Gamma < 1$) combined with relatively low optical/IR extinctions.

One AGN and two AGN candidates: We confirm that IGR J14471–6414 is an AGN based on its positional coincidence with the previously suggested counterpart, which is a Seyfert 1.2 at a redshift of $z = 0.053$ (Masetti et al. 2008). We confirm the association of IGR 19443+2117 with 2MASS and radio counterparts (Landi et al. 2009), but spectral confirmation is still required to confirm that this source is an AGN. Finally, we identify IGR J18485–0047 with a strong radio source. Based on the radio emission and the strong X-ray absorption, we suggest that it may be a Seyfert 2 AGN.

Two SNRs: IGR J14003–6326 and IGR J17448–3232 are both circular extended sources, indicative of being SNRs. In the former case, the putative pulsar appears to be embedded in the SNR, and the hard X-ray emission may be dominated by the PWN. In the latter case, a hard point-like source at the edge of the SNR may indicate that the pulsar was kicked when the explosion occurred. Prior to this work, only 1 IGR source was identified as an SNR, IGR J18135-1751, which has also been detected at TeV energies (Ubertini et al. 2005). The *INTEGRAL* discovery of 2 more SNRs may effect estimates of the hard X-ray emission levels from SNRs in general, and may have implications for the numbers of SNRs that future hard X-ray satellites, such as *NuSTAR* (Harrison et al. 2009) will detect.

Two unclassified sources: We have identified IGR J11098–6457 with CXOU J110926.4–650224 and IGR J18134–1636 with CXOU J181328.0–163548, but the nature of these sources is unclear.

Sources lacking clear counterparts: We did not find clear *Chandra* counterparts for IGR J07295–1329, IGR J09485–4726, IGR J17461–2204, or IGR J17487–3124. This may indicate that these are transient or variable X-ray sources.

JAT acknowledges partial support from *Chandra* award number GO8-9055X issued by the *Chandra X-Ray Observatory Center*, which is operated by the Smithsonian Astrophysical Observatory for and on behalf of the National Aeronautics and Space Administration (NASA), under contract NAS8-03060. JAT would like to thank Michael McCollough for useful conversations about *Chandra* source detection. This publication makes use of data products from the Two Micron

All Sky Survey, which is a joint project of the University of Massachusetts and the Infrared Processing and Analysis Center/California Institute of Technology, funded by NASA and the National Science Foundation. This research makes use of the USNOFS Image and Catalogue Archive operated by the United States Naval Observatory, Flagstaff Station, the SIMBAD database, operated at CDS, Strasbourg, France, and the Deep Near Infrared Survey of the Southern Sky (DENIS).

APPENDIX

The *Chandra* source lists for all 22 observations are available on-line. The lists include sources from the ACIS-I detector only, and the source detection methodology is describe in §3.1. The tables are in the same format as Table 2 with the CXOU *Chandra* name for each source, the angular distance from the center of the *INTEGRAL* error circle, the *Chandra* position, the number of ACIS counts collected in the 0.3–10 keV energy band, and the hardness ratio as defined in §3.1. In a small number of cases near the edges of the detector, background subtraction leads to sources that were detected by `wavdetect` having negative numbers of counts. As we know that some of the `wavdetect` sources are spurious, we removed the sources that have fewer than 1 count. In addition, the tables do not include hardness ratios for sources with fewer than 5 ACIS counts as the errors are too large in these cases. The tables for IGR J07295–1329, IGR J09485–4726, IGR J17461–2204, and IGR J17487–3124 may be especially useful as these were the four sources for which we did not find a clear *Chandra* counterpart. Thus, results from future observations could be compared to the these tables to look for X-ray variability that could help to identify the counterparts of the IGR sources. We note that the 90% confidence *INTEGRAL* error circles for the 4 sources listed above have radii of $5'.4$, $4'.9$, $3'.7$, and $3'.0$, respectively.

REFERENCES

Abdo, A. A., 2009, arXiv:0902.1340 [astro-ph]
Anders, E., & Grevesse, N., 1989, Geochimica et Cosmochimica Acta, 53, 197
Balucinska-Church, M., & McCammon, D., 1992, ApJ, 400, 699
Becker, R. H., White, R. L., Helfand, D. J., & Zoonematkermani, S., 1994, ApJS, 91, 347
Bird, A. J., et al., 2006, ApJ, 636, 765
Bodaghee, A., et al., 2007, A&A, 467, 585
Bozzo, E., Falanga, M., & Stella, L., 2008, ApJ, 683, 1031
Bulgarelli, A., et al., 2009, The Astronomer's Telegram, 2017
Butler, S. C., et al., 2009, ApJ, 698, 502
Cash, W., 1979, ApJ, 228, 939
Chaty, S., Rahoui, F., Foellmi, C., Tomsick, J. A., Rodriguez, J., & Walter, R., 2008, A&A, 484, 783
Dame, T. M., Hartmann, D., & Thaddeus, P., 2001, ApJ, 547, 792
Davis, J. E., 2001, ApJ, 562, 575
Ebisawa, K., et al., 2005, ApJ, 635, 214
Evans, P. A., Beardmore, A. P., & Osborne, J. P., 2008, The Astronomer's Telegram, 1669
Filliatre, P., & Chaty, S., 2004, ApJ, 616, 469
Funk, S., et al., 2007, A&A, 470, 249
Garmire, G. P., Bautz, M. W., Ford, P. G., Nousek, J. A., & Ricker, G. R., 2003, in X-Ray and Gamma-Ray Telescopes and Instruments for Astronomy. Edited by Joachim E. Truemper, Harvey D. Tananbaum. Proceedings of the SPIE, 4851, 28
Gehrels, N., 1986, ApJ, 303, 336
Hands, A. D. P., Warwick, R. S., Watson, M. G., & Helfand, D. J., 2004, MNRAS, 351, 31
Harrison, F., et al., 2009, in American Astronomical Society Meeting Abstracts, Vol. 213, #452.02
Helfand, D. J., Gotthelf, E. V., Halpern, J. P., Camilo, F., Semler, D. R., Becker, R. H., & White, R. L., 2007, ApJ, 665, 1297
Ibarra, A., Kuulkers, E., & Saxton, R., 2008, The Astronomer's Telegram, 1397
in't Zand, J. J. M., 2005, A&A, 441, L1
Kalberla, P. M. W., Burton, W. B., Hartmann, D., Arnal, E. M., Bajaja, E., Morras, R., & Pöppel, W. G. L., 2005, A&A, 440, 775
Keek, S., Kuiper, L., & Hermsen, W., 2006, The Astronomer's Telegram, 810
Kuulkers, E., et al., 2006, The Astronomer's Telegram, 874, 1
Landi, R., et al., 2007a, The Astronomer's Telegram, 1273
Landi, R., Masetti, N., Malizia, A., Bazzano, A., Fiocchi, M., Bird, A. J., & Dean, A. J., 2008a, The Astronomer's Telegram, 1437
Landi, R., et al., 2008b, The Astronomer's Telegram, 1538
Landi, R., et al., 2008c, The Astronomer's Telegram, 1539
Landi, R., et al., 2007b, The Astronomer's Telegram, 1323
Landi, R., et al., 2007c, The Astronomer's Telegram, 1322
Landi, R., et al., 2009, A&A, 493, 893
Lebrun, F., et al., 2003, A&A, 411, L141
Lommen, D., Yungelson, L., van den Heuvel, E., Nelemans, G., & Portegies Zwart, S., 2005, A&A, 443, 231
Malizia, A., et al., 2007, ApJ, 668, 81
Masetti, N., et al., 2008, A&A, 482, 113
Masetti, N., et al., 2009, A&A, 495, 121
Matt, G., & Guainazzi, M., 2003, MNRAS, 341, L13
Negueruela, I., Smith, D. M., Reig, P., Chaty, S., & Torrejón, J. M., 2006, in ESA SP-604: The X-ray Universe 2005, ed. A. Wilson, 165
Parisi, P., Masetti, N., Jimenez, E., Chavushyan, V., Bassani, L., Bazzano, A., & Bird, A. J., 2008, The Astronomer's Telegram, 1710
Rahoui, F., Chaty, S., Lagage, P.-O., & Pantin, E., 2008, A&A, 484, 801
Rodriguez, J., Tomsick, J. A., & Chaty, S., 2009, A&A, 494, 417
Sguera, V., et al., 2006, ApJ, 646, 452
Steeghs, D., Knigge, C., Drew, J., Unruh, Y., & Greimel, R., 2008, The Astronomer's Telegram, 1653
Sugizaki, M., Mitsuda, K., Kaneda, H., Matsuzaki, K., Yamauchi, S., & Koyama, K., 2001, ApJS, 134, 77
Tomsick, J. A., 2009, The Astronomer's Telegram, 2022
Tomsick, J. A., Chaty, S., Rodriguez, J., Foschini, L., Walter, R., & Kaaret, P., 2006, ApJ, 647, 1309
Tomsick, J. A., Chaty, S., Rodriguez, J., Walter, R., & Kaaret, P., 2008a, ApJ, 685, 1143
Tomsick, J. A., Chaty, S., Rodriguez, J., Walter, R., Kaaret, P., & Tovmassian, G., 2009, ApJ, 694, 344
Tomsick, J. A., et al., 2008b, ApJ, 680, 593
Tomsick, J. A., Rodriguez, J., Chaty, S., Walter, R., & Kaaret, P., 2008c, The Astronomer's Telegram, 1649
Ubertini, P., et al., 2005, ApJ, 629, L109
Ubertini, P., et al., 2003, A&A, 411, L131
Vercellone, S., et al., 2009, The Astronomer's Telegram, 2019
Walter, R., et al., 2003, A&A, 411, L427
Walter, R., & Zurita Heras, J., 2007, A&A, 476, 335
Walter, R., et al., 2006, A&A, 453, 133
Weisskopf, M. C., 2005, arXiv:astro-ph/0503091
Wilms, J., Allen, A., & McCray, R., 2000, ApJ, 542, 914
Winkler, C., et al., 2003, A&A, 411, L1